

Ultrafast tunable modulation of light polarization at THz frequencies

Vincent Juvé,* Gwenaëlle Vaudel, Vasily Temnov, and Thomas Pezeril

*Institut des Molécules et Matériaux du Mans, UMR CNRS 6283,
Université du Maine, avenue Olivier Messiaen, 72085 Le Mans, France*

Zoltan Ollmann and Janos Hebling

*Department of Experimental Physics and MTA-PTE High Field
Terahertz Research Group, University of Pécs, 7624 Pécs, Hungary*

Vitalyi Gusev

*Laboratoire d'Acoustique de l'Université du Maine, UMR CNRS 6613,
Université du Maine, avenue Olivier Messiaen, 72085 Le Mans, France*

(Dated: November 7, 2017)

PACS numbers:

Controlling light polarization is one of the most essential routines in modern optical technology. Since the demonstration of optical pulse shaping by spatial light modulators^{1,2} and its potential in controlling quantum reaction path³, it paved the way to many applications⁴ as coherent control of photoionization process^{5,6}, space-time control of propagating phonons⁷ or as polarization shaping of Terahertz (THz) pulses⁸. Here we evidenced efficient non-resonant and noncollinear $\chi^{(2)}$ -type light-matter interaction in femtoseconds polarization sensitive time-resolved optical measurements. Such nonlinear optical interaction of visible light and ultra-short THz pulses leads to THz modulation of visible light polarization in bulk LiNbO₃ crystal. Theoretical simulations based on the wave propagation equation capture the physical processes underlying this astonishing effect. Apart from the observed tunable polarization modulation at ultra-high frequencies of visible pulses, this new physical phenomenon can be envisaged in THz depth-profiling of materials.

Over the last decade, ultrafast Terahertz spectroscopy has gained tremendous attention thanks to the development of high-power ultrafast laser systems⁹, which allowed to generate intense single-cycle picosecond pulses of electric field at THz frequencies^{10,11}. Their relatively long cycle period (1 ps for 1 THz) and high electric field (from hundred of kV/cm to few MV/cm) provide a new

tool for studying fundamental aspects of light-matter interactions like THz-driven ballistic charge currents in semiconductors^{12,13}, linear¹⁴ and nonlinear¹⁵ control of antiferromagnetic spin waves, THz-induced dynamics in metallic ferromagnets¹⁶ and transparent magneto-optical media¹⁷, or even an ultrafast switching of electric polarization in ferroelectrics¹⁸.

Despite of this explosive development of THz spectroscopy, studies on phase-matched second-order nonlinear optical interactions between THz and visible pulses are rare and only up-conversion of THz pulses were used for THz pulse characterization¹⁹. Phase-matched propagation of THz and visible pulses is expected to lead to an efficient ordinary-to-extraordinary conversion for visible photons at approximately the same frequency, $\hbar\omega_e = \hbar\omega_o \pm \hbar\omega_o^{\text{THz}} \simeq \hbar\omega_o$. This would lead to a large polarization change of the optical pulse. Since non-resonant THz-induced optical nonlinearities in dielectric crystals are nearly instantaneous, the magnitude of the polarization change should be determined solely by the spatio-temporal dynamics of interacting THz and visible pulses propagating inside the crystal and, thus, the polarization switching time lies in the range of few terahertz governed by the pulses duration involved. In other words, such non-resonant nonlinear optical interactions set the fundamental speed limits of electro-optical modulation, which is limited to gigahertz switching time for conventional devices²⁰.

Here we report on femtoseconds time-resolved THz pump-optical probe experiments, where an intense THz pump and a visible probe pulse interact during their propagation inside the LiNbO₃ crystal (see Methods). Optical properties of visible probe pulses are monitored by polarization sensitive measurements (rotation and ellipticity) as a function of the pump-probe delay time. Two distinct (front-side and back-side) probing configurations are sketched in Fig. 1 (a) and in the inset of Fig. 1 (b), respectively. The THz electric field amplitude on the sample is in the order of 100 kV/cm.

Fig. 1 (b) shows a typical pump-probe transient measured in the back-side probing configuration at 400 nm probe wavelength and $\alpha_{\text{in}} = 10^\circ$ ($\alpha_{\text{out}} = 25^\circ$). Due to the polarization-sensitive detection scheme with a half waveplate (H.W.P.), the measured signal is linked to the rotation of the polarization state of the visible probe pulses induced by nonlinear optical interaction with the THz pulses propagating in the crystal and exhibits time domain oscillations at two distinct frequencies of 0.22 THz (low frequency ν_-) and 0.69 THz (high-frequency ν_+), respectively. For this particular experimental configuration, the rotation angle, denoted as the polarization rotation angle $\Delta\theta$, is approximately 1° , which corresponds to a polarization conversion efficiency of $\sim 5\%$. The same signal amplitude is observed when measuring the ellipticity change with a quarter waveplate

(Q.W.P.) shown by the inset of Fig. 4). The occurrence of high frequency ν_+ and low frequency ν_- can be uniquely attributed to co- and counter-propagating THz and visible pulses, respectively. The frequency changes from high to low and vice-versa each time the THz pulse is reflected at one of the crystal surfaces. Switching from front-side to back-side probing geometries while keeping the angle α_{in} constant naturally leads to the exchange of the high and low frequency parts of optical signal (not shown). The alternating time windows for the observation of co- and counter-propagating THz and visible pulses inside the crystal of thickness L (see Fig 1 (b)) are governed by group velocities:

$$\Delta\tau_+ \approx \frac{L}{c}(n_{\text{THz}} - n_0^{\text{gr}}) \text{ and } \Delta\tau_- \approx \frac{L}{c}(n_{\text{THz}} + n_0^{\text{gr}}), \quad (1)$$

with n_0^{gr} the visible light group index (polarized along the ordinary axis) and $n_{\text{THz}}^{\text{gr}} = n_{\text{THz}}$ the refractive index of the THz pulse, considering that the LiNbO₃ is not dispersive in this frequency range. The different time intervals $\Delta\tau_{+,-}$ are experimentally found to be 12.1 ps and 32.3 ps, and, considering the value of the visible group refractive index, one can extract the THz ordinary refractive index $n_{\text{THz}} \approx 6.75$, which is in good agreement with the literature^{21,22}. Finally the signal duration of hundreds of picoseconds and the drops in amplitude for each reflection at the interfaces are explained by the absorption coefficient of the LiNbO₃ in the THz spectral range and by the THz reflection coefficient, which is roughly 75% for the field amplitude.

Measurements at different probe angles α_{in} ranging from 0 to 16° have been performed and are displayed in Fig. 1 (c) for a probe's wavelength $\lambda_0 = 400$ nm. The curve at 0° reflects the result one can obtain by doing a non phase-matched electro-optic sampling measurement in a crystal (in ZnTe for instance²³), when signal originates only at the interfaces. On top of this effect, noncollinear geometry gives birth to the single low and high frequencies, which increase continuously as a function of the angle α_{in} . The relative amplitudes of the signals will be discussed later.

Systematic investigation of the evolution of the observed frequencies versus the probe angles α_{in} and for two wavelengths $\lambda_0 = 400$ nm and $\lambda_0 = 800$ nm was carried out and is displayed in Fig. 2. For each wavelength, two frequency branches (ν_+ and ν_-) appear, which correspond to co- and counter- propagating THz and visible pulses as described previously. The maximum measured frequency is 1.6 THz ($\alpha_{\text{in}} \approx 15^\circ$) for $\lambda_0 = 400$ nm and 1.1 THz ($\alpha_{\text{in}} \approx 22^\circ$) for $\lambda_0 = 800$ nm. Dashed lines correspond to the results of the theoretical solution based on our model, which is described in details in the Supplementary Materials, and are perfectly in agreement with experimental results.

For a quantitative insight into the nonlinear process involved here, we have measured the amplitude of the change of the light's polarization angle $\Delta\theta$ while sweeping the internal angle α_{in} for a wavelength of 400 nm. In Fig. 3, $\Delta\theta$ of the first occurring oscillations (ν_+ or ν_-) is plotted as a function of the frequencies for the two experimental configurations namely the front-side and back-side probing geometries. The first striking feature is the measured maximum polarization rotation angle, occurring at 0.6 THz for the ν_+ , which is as high as 6° . This corresponds to a light polarization conversion efficiency of 20% upon the presence of the THz pulse. This particularly large light's polarization rotation angle is the largest reported so far in the literature, which are rather small in the order of one degree in ultrafast experiments^{16,24}. The second striking feature is the difference in the maximum rotation angle for ν_+ and ν_- with a almost factor of 3 higher amplitude for ν_+ . Along with the experimental data points, the results of numerical evaluation of the analytical theoretical prediction of time integration of Eq. S18 is plotted for both co- (ν_+) and counter-propagating (ν_-) pulses. These are in a good agreement with the experimental results. Moreover, the spectral amplitude of the polarization rotation transients are proportional to the spectral components of the THz pulse used in the experiments shown in dashed line in Fig. 3. In the light of these results, the main effect of tuning the angle is to fulfill the phase matching condition for the different frequency component contained in the pump THz spectrum, which directly lead to the THz pulse sampling in the frequency domain, and, thus, allow to adjust the modulation frequency of the probe pulse (see Supplementary Materials for explicit phase matching conditions).

The experimental results were analyzed by theoretical simulations of the scattering process between the light and THz pulses within the sample. We considered second-order nonlinear interaction between the electric field of the ordinary polarized THz pulse and of the ordinary polarized visible probe, leading to the generation of an extraordinary optical beam. Solving the wave propagation equation for the extraordinary beam generated by this interaction in our experimental configuration leads to the establishment of the signal amplitude as the function of the time delay τ between the THz pump and the optical probe beam, which is governed by an interplay between distinct phase and group-matching conditions for visible and THz electromagnetic fields (see Supplementary Information and Eqs. S17 and S18).

In our model, we only consider the second order nonlinear effect occurring in the bulk of the crystal and the particular case of $\alpha_{\text{in}} = 0^\circ$ cannot be simulated. In the simulations, there is no free parameters; the model's inputs are only related to the parameters of the material and of the

pulse, which are determined independently. Nevertheless the simulated transients are in a very good agreement with the experimental ones as we included the reflection coefficient as well as the THz absorption of the crystal (see Fig. S2). The computed frequencies of the oscillations versus the angle α_{in} are displayed in dashed lines in the figure 2 and perfectly agree the experimental observation for two different wavelengths. There is as well a good agreement between the calculated and measured amplitudes of the oscillations, which are displayed in figure 3 with only a scaling factor. It is interesting to note that the ratio of the v_+ and v_- simulated amplitudes is frequency independent and is equal to 2.7. This ratio can be explained by the longer interaction time of the THz pulse with the co-propagating light field than with the counter-propagating one, $\left(\frac{n_{\text{THz}} + n_{\text{o}}^{\text{gr}}}{n_{\text{THz}} - n_{\text{o}}^{\text{gr}}}\right) = 2.7$, agreeing with the experimental value of ≈ 3 . Deviation of the numerical simulation starting at around 0.4 THz for the back-side configuration, corresponding to an angle $\alpha_{\text{in}} \approx 15^\circ$ ($\alpha_{\text{out}} \approx 38^\circ$), can be explained by the geometrical effect of the beams crossing in the sample which is neglected in our model.

We now discuss the physical effect underlying the THz controlled polarization rotation of the visible probe pulse. The signal originates from two different physical effects governed by the $\chi^{(2)}$ susceptibility tensor: electro-optic effect, which occurs at the sample's surfaces when both the THz pump and the visible probe are overlapped in time, and phase-matched nonlinear interaction, which occurs in the bulk. The former effect, which is non-resonant and broadband, results from a change in the refractive index caused by the THz pulse at the surface: the measured temporal transient is then related to the actual temporal shape of the THz pulse, leading to the sampling in time of the THz pulse by the light pulse. The effect exists both for collinear^{25,26} and noncollinear²⁷ propagation of the THz and light pulses. This technique, free-space electro-optic sampling, is widely used since decades in linear and non-linear THz spectroscopy²⁸. The latter effect relies on the phase and group-matching conditions (see Eqs S17 and S18), which takes place within the sample only for the noncollinear propagation of the THz and light pulses, and can be adjusted by tuning the angle between the two incident beams. This leads to an angle-selectivity of each frequency component contained in the THz pulse and, by sweeping the angle, one can retrieve the THz spectrum as shown in figure 3.

One potential application would be to use picosecond pulses of visible light roughly equal to $\Delta\tau_-$ or $\Delta\tau_+$. This configuration would lead to an ultrafast periodic modulation of the polarization state of the visible light at THz frequency, depending on the crossing angle α_{in} between THz and optical pulses. An example of such shaped pulse is displayed in Fig. 4. As the modulation fre-

quency can be modified easily it can be tuned to resonantly drive systems like coherent THz optical phonon excitation in solids^{29,30} and active Raman-active media⁴ for example. Another possible application of our experimental scheme is to add the third (axial) coordinate to the well-known 2D imaging with THz waves^{31–34}, which currently provides only lateral resolution. The micrometer axial resolution for depth-profiling of the suggested three-dimensional imaging technique (see Supplementary Materials) is controlled by the spatial overlap of the THz and probe light pulses and, in case of their counter-propagation, could outperform the echography with THz pulses³⁵.

In conclusion, we have experimentally demonstrated an ultrafast tunable polarization modulation of a light pulse at a wavelength of 400 nm and 800 nm caused by non-resonant interaction with an ultrashort THz pulse in LiNbO₃ crystal. This effect originates from $\chi^{(2)}$ -type noncollinear interactions between optical and THz electromagnetic pulses and occurs in the bulk of the crystal. For a given set of optical wavelengths, using a noncollinear configuration, it is possible to select a narrow frequency band of the light's polarization modulation within the THz frequency spectrum by adjusting the angle between the two pulses. The maximum polarization rotation and ellipticity was measured to be $\sim 6^\circ$ and $\sim 15\%$ at the internal angle of $\sim 8.5^\circ$ between the THz pulse and a 400 nm visible probe. This new phenomenon is modeled by solving the wave propagation equation. Analytical expressions (Eqs. S17 and S18) show that an interplay between distinct phase and group-matching conditions for visible and THz electromagnetic fields determines the overall conversion efficiency. Being in excellent agreement with theoretical calculations, our experimental findings establish the fundamental limits of electro-optical modulation speed and open the door to the design of ultrafast miniaturized electro-optical devices for pulse shaping operating in the multi-THz range.

Methods

Experimental setup

Both pump and probe pulses are generated by an amplified Ti:sapphire laser system (pulse energy 3 mJ and duration 120 fs, central wavelength 800 nm, repetition rate 1 kHz). The main fraction of the laser is used to generate ultrashort THz pulses by optical rectification in a stoichiometric MgO-doped LiNbO₃ crystal by the tilted pulse front method^{10,11,36}. Single cycle THz pulses with a duration of around 1.6 ps (full width half maximum), a pulse energy of roughly

$1\mu J$ and a spectrum centered at 0.5 THz spanning frequencies from 0.2 to more than 1.5 THz are measured by electro-optic sampling technique with a $\langle 110 \rangle$ ZnTe crystal²³ (see Fig. 3 dashed line and figure 4 of the Supplementary Information). The pump pulse is mechanically chopped (500 Hz), and the generated THz pulse is focused by an off axis parabolic mirror and overlapped together with the probe pulse in the sample (undoped z-cut LiNbO₃ crystal of 1 mm thickness). The remaining fraction is used as probe pulses at 800 nm or 400 nm wavelength obtained through frequency doubling in a BBO-crystal. The THz pulse impinges the sample at normal incidence and the probe's incident angle α_{out} (α_{in}) can be tuned from 0 to roughly 60° (25°) outside (inside) the sample, respectively. Both polarizations are ordinary. After passing through the sample, the probe's change of polarization (rotation and ellipticity) is detected by a half waveplate or a quarter waveplate, a Wollaston prism and a balanced photodiode connected to a lock-in amplifier. The signal output is then expressed by $\Delta I/I = (I_{\text{PD1}} - I_{\text{PD2}})/(I_{\text{PD1}} + I_{\text{PD2}})$, with $I_{\text{PD1,2}}$ the light power in each photodiode.

Acknowledgments

The IMMM's group acknowledges fruitful discussions with Prof. P. Ruello. V.J. acknowledges Campus France and the Région Pays de la Loire through the NNN-Telecom and Echopico projects. The experiments were implemented on the fs laser platform of IMMM.

Authors contributions

T.P. initiated the project. Z.O., J. H., G. V. and T. P. built the THz source. V.J., G.V. conducted the experiments. V.J., G.V. carried out the data analysis. V.G. derived the theoretical framework, from which V.G., V.J. and V.T. interpreted the data while V.J. performed numerical evaluations. V.J. wrote the manuscript, to which all authors suggested improvements and agree to its content.

* `vincent.juve@univ-lemans.fr`

¹ A. M. Weiner, J. P. Heritage, and E. Kirschner, *JOSA B* **5**, 1563 (1988).

² A. M. Weiner, *Review of scientific instruments* **71**, 1929 (2000).

³ R. S. Judson and H. Rabitz, *Physical Review Letters* **68**, 1500 (1992).

- ⁴ K. Misawa, *Advances in Physics: X* **1**, 544 (2016).
- ⁵ T. Brixner, G. Krampert, T. Pfeifer, R. Selle, G. Gerber, M. Wollenhaupt, O. Graefe, C. Horn, D. Liese, and T. Baumert, *Physical review letters* **92**, 208301 (2004).
- ⁶ G. Vogt, G. Krampert, P. Niklaus, P. Nuernberger, and G. Gerber, *Physical review letters* **94**, 068305 (2005).
- ⁷ T. Feuerer, J. C. Vaughan, and K. A. Nelson, *Science* **299**, 374 (2003).
- ⁸ M. Sato, T. Higuchi, N. Kanda, K. Konishi, K. Yoshioka, T. Suzuki, K. Misawa, and M. Kuwata-Gonokami, *Nature Photonics* **7**, 724 (2013).
- ⁹ T. Kampfrath, K. Tanaka, and K. A. Nelson, *Nature Photonics* **7**, 680 (2013).
- ¹⁰ K.-L. Yeh, M. Hoffmann, J. Hebling, and K. A. Nelson, *Applied Physics Letters* **90**, 171121 (2007).
- ¹¹ H. Hirori, A. Doi, F. Blanchard, and K. Tanaka, *Applied Physics Letters* **98**, 091106 (2011).
- ¹² W. Kuehn, P. Gaal, K. Reimann, M. Woerner, T. Elsaesser, and R. Hey, *Physical review letters* **104**, 146602 (2010).
- ¹³ O. Schubert, M. Hohenleutner, F. Langer, B. Urbanek, C. Lange, U. Huttner, D. Golde, T. Meier, M. Kira, S. W. Koch, *et al.*, *Nature Photonics* **8**, 119 (2014).
- ¹⁴ T. Kampfrath, A. Sell, G. Klatt, A. Pashkin, S. Mährlein, T. Dekorsy, M. Wolf, M. Fiebig, A. Leitenstorfer, and R. Huber, *Nature Photonics* **5**, 31 (2011).
- ¹⁵ S. Baierl, M. Hohenleutner, T. Kampfrath, A. Zvezdin, A. Kimel, R. Huber, and R. Mikhaylovskiy, *Nature Photonics* (2016).
- ¹⁶ C. Vicario, C. Ruchert, F. Ardana-Lamas, P. M. Derlet, B. Tudu, J. Luning, and C. P. Hauri, *Nature Photonics* **7**, 720 (2013).
- ¹⁷ R. Subkhangulov, R. Mikhaylovskiy, A. Zvezdin, V. Kruglyak, T. Rasing, and A. Kimel, *Nature Photonics* (2016).
- ¹⁸ R. Mankowsky, A. von Hoegen, M. Först, and A. Cavalleri, *Physical Review Letters* **118**, 197601 (2017).
- ¹⁹ S. Hayashi, K. Nawata, T. Taira, J.-i. Shikata, K. Kawase, and H. Minamide, *Scientific reports* **4**, srep05045 (2014).
- ²⁰ Y.-q. Lu, M. Xiao, and G. J. Salamo, *Applied Physics Letters* **78**, 1035 (2001).
- ²¹ M. Schall, H. Helm, and S. Keiding, *International journal of infrared and millimeter waves* **20**, 595 (1999).
- ²² M. Unferdorben, Z. Szaller, I. Hajdara, J. Hebling, and L. Pálfalvi, *Journal of Infrared, Millimeter, and*

- Terahertz Waves **36**, 1203 (2015).
- ²³ P. C. Planken, H.-K. Nienhuys, H. J. Bakker, and T. Wenckebach, *JOSA B* **18**, 313 (2001).
- ²⁴ R. V. Mikhaylovskiy, R. R. Subkhangulov, T. Rasing, and A. V. Kimel, *Optics letters* **41**, 5071 (2016).
- ²⁵ M. Van Exter, C. Fattinger, and D. Grischkowsky, *Applied Physics Letters* **55**, 337 (1989).
- ²⁶ Q. Wu and X.-C. Zhang, *Applied Physics Letters* **67**, 3523 (1995).
- ²⁷ J. Shan, A. S. Welington, E. Knoesel, L. Bartels, M. Bonn, A. Nahata, G. A. Reider, and T. F. Heinz, *Optics letters* **25**, 426 (2000).
- ²⁸ D. Grischkowsky, S. Keiding, M. Van Exter, and C. Fattinger, *JOSA B* **7**, 2006 (1990).
- ²⁹ K. Sokolowski-Tinten, C. Blome, J. Blums, A. Cavalleri, C. Dietrich, A. Tarasevitch, I. Uschmann, E. Förster, M. Kammler, M. Horn-von Hoegen, *et al.*, *Nature* **422**, 287 (2003).
- ³⁰ D. M. Fritz, D. Reis, B. Adams, R. Akre, J. Arthur, C. Blome, P. Bucksbaum, A. L. Cavalieri, S. Enge-
mann, S. Fahy, *et al.*, *Science* **315**, 633 (2007).
- ³¹ B. Hu and M. Nuss, *Optics letters* **20**, 1716 (1995).
- ³² Q. Wu, T. Hewitt, and X.-C. Zhang, *Applied Physics Letters* **69**, 1026 (1996).
- ³³ M. C. Nuss, *IEEE Circuits and Devices Magazine* **12**, 25 (1996).
- ³⁴ A. Fitzgerald, E. Berry, N. Zinovev, G. Walker, M. Smith, and J. Chamberlain, *Physics in Medicine and
biology* **47**, R67 (2002).
- ³⁵ J. B. Jackson, J. Labaune, R. Bailleul-Lesuer, L. DAlessandro, A. Whyte, J. W. Bowen, M. Menu, and
G. Mourou, *Frontiers of Optoelectronics* **8**, 81 (2015).
- ³⁶ J. Hebling, A. Stepanov, G. Almási, B. Bartal, and J. Kuhl, *Applied Physics B* **78**, 593 (2004).

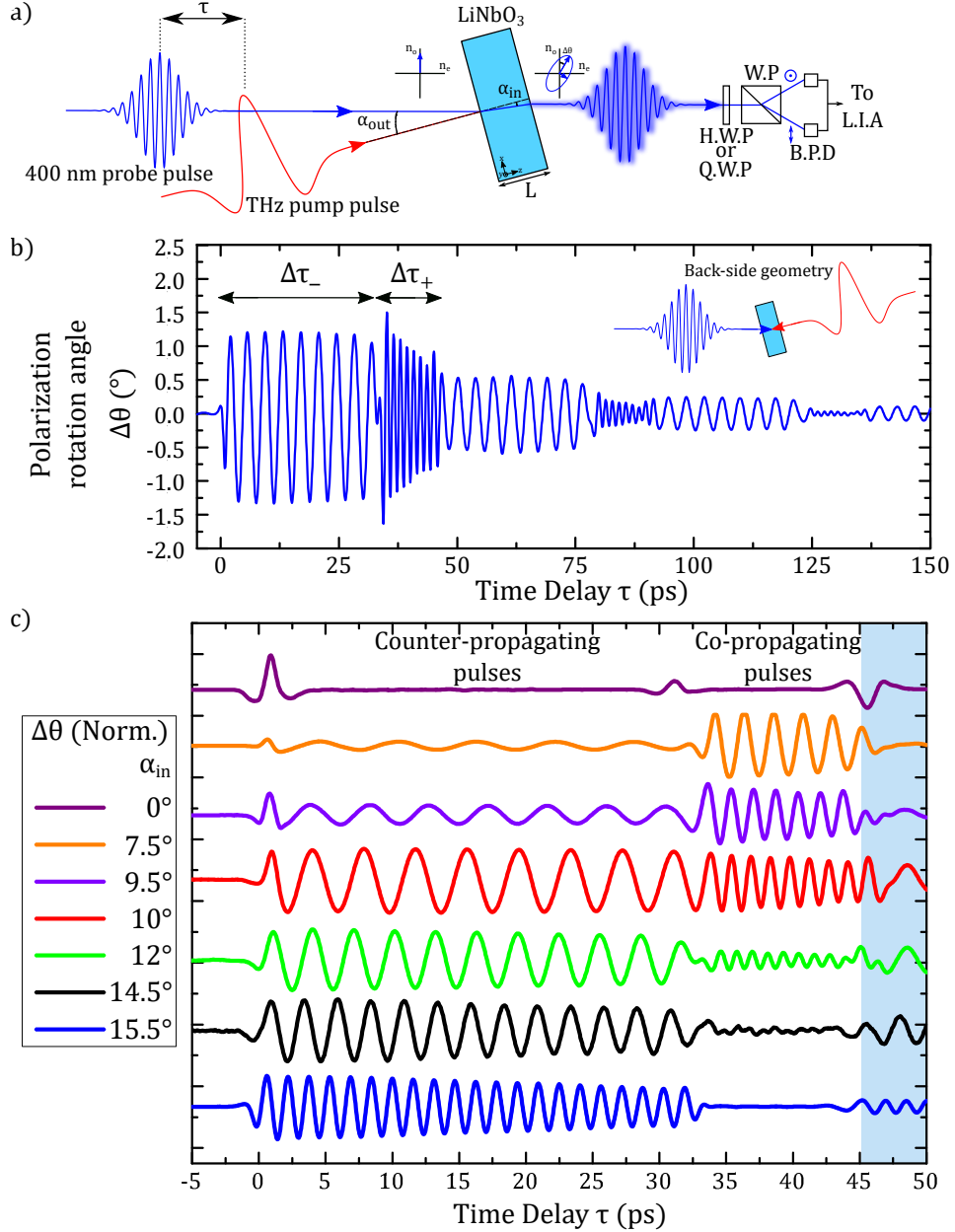


FIG. 1: Terahertz-induced light's polarization change: experimental geometry and results. (a) Schematic of the time-resolved polarization change measurement in a z-cut LiNbO₃ crystal in the front-side probing configuration. Half Waveplate (HWP) and Quarter Waveplate (QWP) can be used to measure the polarization rotation and ellipticity changes, respectively. W.P.: Wollaston Prism. B.P.D: Balanced Photo-Diodes. L.I.A: Lock-In Amplifier. L: sample's thickness. (b) Relative change of the probe light polarization orientation as a function of the time delay τ between the THz pump pulse and the 400 nm probe pulse for $\alpha_{out} = 25^\circ$ ($\alpha_{in} = 10^\circ$) in the back-side probing configuration, shown by the small sketch. (c) Ultrafast transients obtained for different probe angles as a function of the time delay between the pump and the probe in the back-side probing configuration. The curves are normalized and shifted for the sake of clarity.

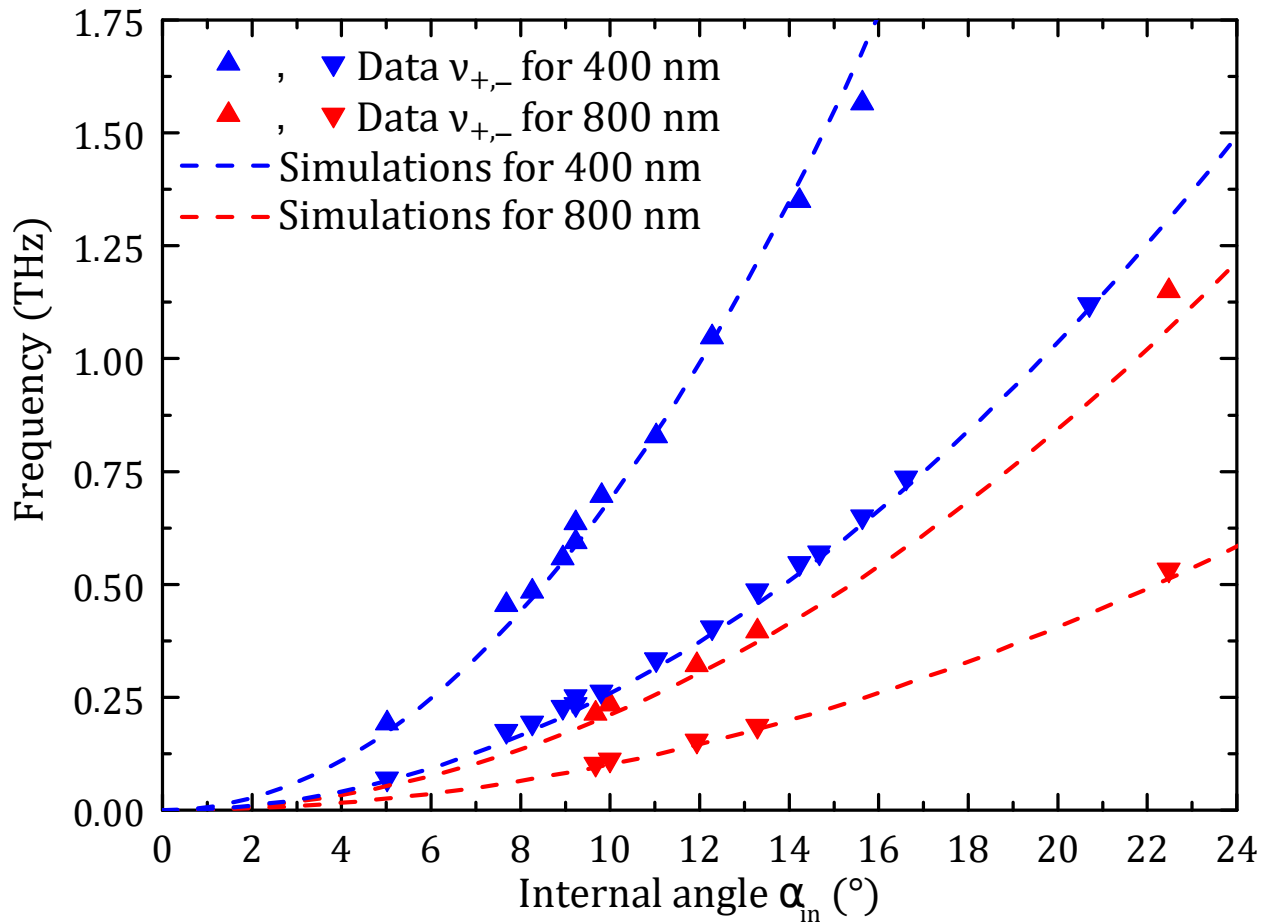


FIG. 2: **Measured frequencies as a function of the probe's incidence angle.** Two different wavelengths $\lambda_0 = 400$ nm (blue triangles) and $\lambda_0 = 800$ nm (red triangles) are plotted as well as the predictions of our model for both wavelengths (dashed lines).

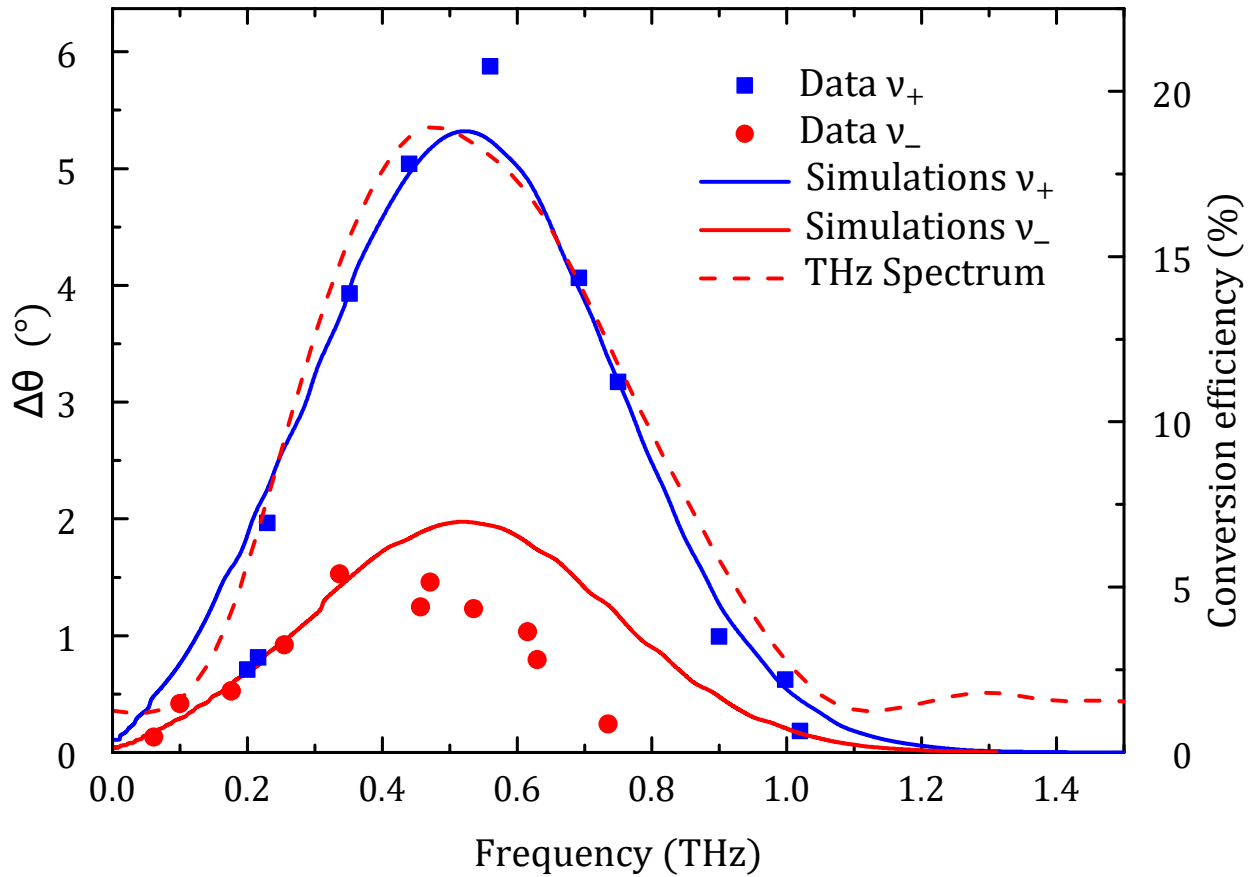


FIG. 3: **Polarization rotation angle as a function of the measured frequency.** Comparison of experimental oscillatory signals as a function of their frequency for the High Frequency (squares) and the Low Frequency (dots) modes for a 400 nm wavelength. Simulations based on the numerical evaluation of time integration of Eq S18 are displayed in solid lines. For comparison, the experimental THz spectrum is shown in dashed line.

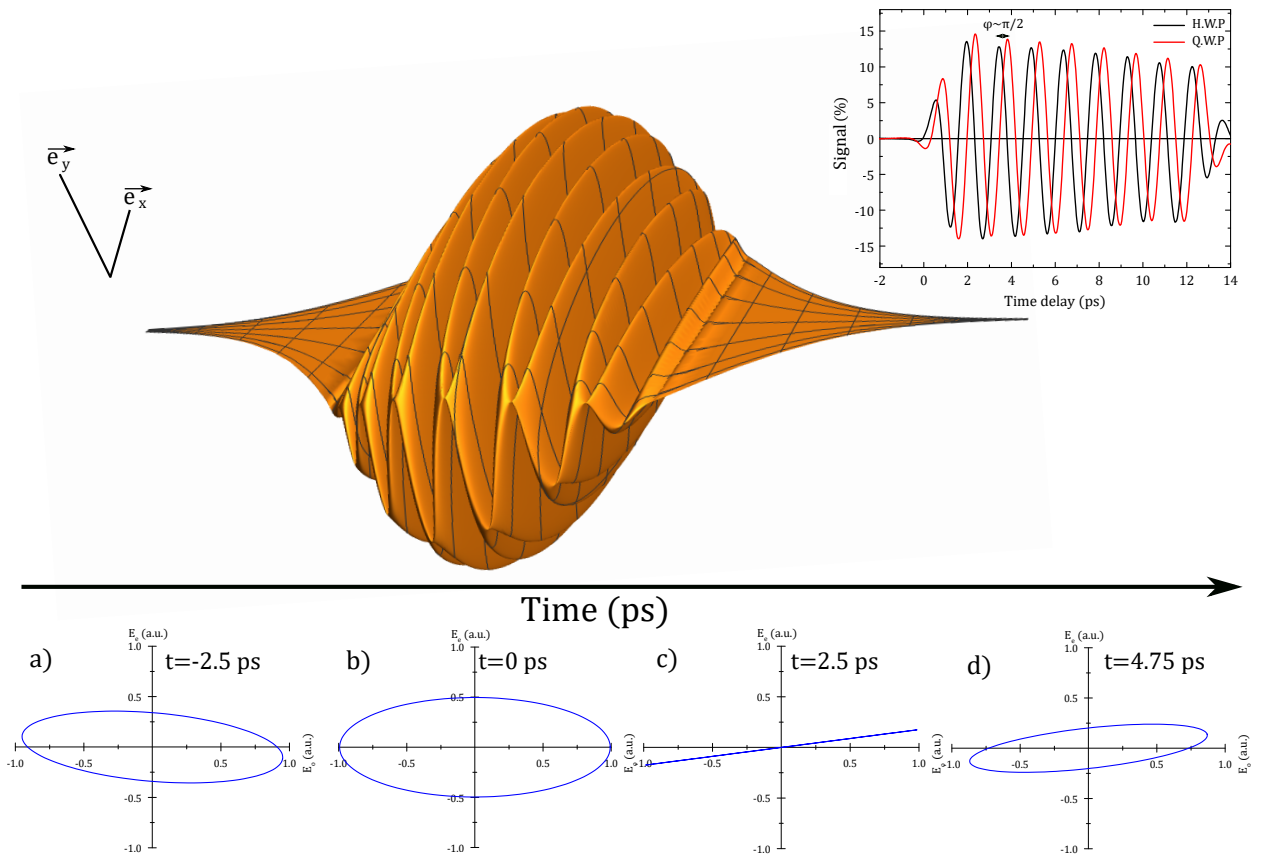


FIG. 4: **Three dimensional representation of the envelope of a polarization shaped optical pulse by nonlinear interaction with a THz pulse in a LiNbO₃ crystal for an optical pulse duration of 15 ps.** The pulse envelop is defined by $\vec{A}(t) = A_o(t)\tilde{e}_x + A_e(t)\tilde{e}_y$ (see the Supplementary Materials). The polarization modulation frequency is 0.5THz, the maximum polarization rotation is 10° and the maximum ellipticity is 0.5. The value of the ellipticity change was blown up for sake of clarity. a) to d) represent the instantaneous light's polarization state for different times. Inset: Experimental transient of the rotation and ellipticity relative changes of the probe pulse for an angle $\alpha_{in} \sim 9^\circ$ and $\lambda = 400$ nm.